SPECTRAL PROPERTIES OF CHLOROPHYLLS IN EDIBLE PLANTS INTENDED FOR DIAGNOSTICS

A. PELED[#], SIMONA ALEXANDRA POPESCU

https://www.doi.org/10.59277/RJB.2024.2.01

Photonics Laboratory, Holon Institute of Technology, 52 Golomb Str., Holon, 5867910, Israel,
[#]e-mail: peled@hit.ac.il

Abstract. This study examined the absorption and fluorescence spectra of chlorophylls and other pigments extracted in ethanol solutions from common edible plant species. Chlorophyll-a was the dominant fluorescent chromophore in all plant varieties. The fluorescence curves for all extracted solutions exhibit after optimizing by concentration dilution an increase in the fluorescence with a typical prominent leading Gaussian peak at a wavelength of 674 nm. This peak is followed by a decreasing shoulder extending into the near-infrared range beyond 724 nm. The dilution of the solutions with ethanol reduces the optical absorption from the other pigments and shows simultaneously an improved resolution of the chlorophyll-a spectral absorption peaks. This investigation provides new insights into the optical absorbance and other photo-excited processes that impact the fluorescence of chlorophylls, such as agglomeration, photobleaching and photo-aggregation. The findings may be used for bio-diagnostics, fluorescent quantum dots and bio-sensors.

Key words: Chlorophyll, spectral analysis, intrinsic fluorescence.

INTRODUCTION

The sensitive detection of biomolecules is very important in many bioengineering applications. Chlorophyll pigments, for instance, have found uses in bio-technological fields such as medical diagnostics and the development of new materials for bio-devices [1, 23]. Since chlorophyll-a (Chl-a) is a key molecule in photosynthesis, its properties have been studied extensively *in vivo* and *in vitro* for many years [5, 9, 16, 24]. However, specific details on the fluorescence of the Chl-a molecule per se, dissolved in simple solutions other than those related to photosynthesis, are still not quite abundant, and thus difficult to compare [10, 26]. In fact, a comprehensive understanding of Chl-a spectra mechanisms in specific solutions such as ethanol is very hard to conclude from the vast information scattered in the literature in so many partially overlapping sub-domains [26]. This has resulted

Received: December 2023;
in final form January 2024.

in overlooking how dilution affects the fluorescence efficiency of Chl-a molecules in non-toxic solvents such as ethanol. Fortunately, it is easier to characterize this molecule in these solvents as compared to leaves, which are bound to protein complexes and membranes that complicate the interpretation of their spectral properties. Diluted Chl-a solutions can also be easily combined with other chromophores from plants and other organic or even inorganic materials to investigate new applications such as amplified stimulated emission (ASE), which can be used to create new types of lasers and efficient solar cells [2, 4].

MATERIALS AND METHODS

Twenty edible plants, namely: *Artemisia arborescens*, spinach, sage, chives, mentha, parsley, celery, dill, mangold, beet greens, coriander, rosemary, lettuce, leek, green cabbage, rocket, basil, green onion, sorrel and red cabbage were purchased from the market and used in this research. Ethanol of 95 % purity was used as the solvent for obtaining the chlorophyll solutions.

CHLOROPHYLL EXTRACTION

The as extracted chlorophyll (Chl) solutions were prepared by mixing standard batches of 10 g ground leaves with 30 mL of 95 % ethanol. Ethanol was chosen because it is non-toxic, completely soluble in water, and a good solvent for organic materials such as chlorophylls, which are inherently quite hydrophobic [20]. The ground wet slurry was filtered at room temperature (25 ºC) using Whatman filter paper No. 1, to obtain clear chlorophyll solutions. The solutions were then stored in the dark at 5 ºC until optical spectral experiments were conducted at room temperature. Standard 3.6 mL volume solutions were used for the spectral experiments. The as-extracted Chl solutions concentrations, denoted as C1, were further diluted with the same ethanol solvent in 7 steps, to also obtain a whole range of lower chromophores concentrations according to the following procedure. The C2 diluted concentrations were obtained by combining 1/2 of the volume of the C1 solutions i.e. 1.8 mL with additional 1.8 mL 95 % pure ethanol. By repeating this consecutive dilution method 6 more times, we obtained even lower concentration solutions denoted as C3–C8. The absolute actual concentrations in μg/cc were finally obtained from the spectral optical density measurements of each solution sample.

SPECTRA ACQUISITION

A Pasco Spectrometer system model 2600, equipped for both optical absorbance and fluorescence measurements, was employed. The fluorescence measurements were conducted by the optical orthogonal method with a blue-violet LED exciting source of 405 nm peak wavelength, bandwidth of 5 nm, and maximum power of 40 mW. The photodetection system had an overall spectral resolution of 2

nanometers. The measuring system was connected to a PC with specific software for calibrating, measuring, and processing the raw acquired spectra.

For the spectral experiments, polymethylmethacrylate (PMMA) standard cuvettes with an optical path length of 1 cm were used. The cuvettes are transparent throughout the spectrum band of 350–800 nm, with an absorbance of less than optical density (*OD*) = 0.001. The standard volume samples of 3.6 mL were taken for each spectral run. Stabilized steady-state optical absorption and fluorescence measurements were carried out in the whole VIS-NIR optical spectral range.

As explained above C1 denotes the extracted solutions samples and their concentrations. The diluted samples with the highest measured fluorescence are denoted as Copt and the most diluted ones as C8. It was observed that during the spectral steady-state measurements, the fluorescent signal increases monotonically up to a maximum level. A quasi-steady state then follows during which the fluorescence level is constant. After a prolonged exposure to the exciting light, the fluorescence decreases to lower levels due to photobleaching and photo-aggregation effects, observed also elsewhere [27]. To obtain reproducible results, a protocol was used where the fluorescence was captured exactly at its maximum level, occurring typically within 40–60 seconds. All measurements were performed with an integration time of 800 msec and averaging 20 scans per sample.

RESULTS AND DISSCUSSION

OPTICAL ABSORPTION AND FLUORESCENCE SPECTROSCOPY

In this section we present the experimental results of the absorbance and fluorescence spectra for the 3 representative Chl concentrations designated as C1, Copt and C8 of all 20 plants. Table 1 shows the typical concentrations C1 of the various chromophores calculated from the absorbance spectra of all plants in the as extracted solutions. The concentration of the specific chromophores present in the solutions was estimated using the Beer-Lambert law from the actual optical density (*OD*) of the main pigments' absorption peak lines using their extinction coefficients ε ($mol^{-1}cm^{-1}$) taken from similar ethanol-based solutions published in the literature [7, 10, 15]. The following molar extinction coefficients at the specific main peaks were used: 83,890 ($mol^{-1}cm^{-1}$) at 432 nm for Chl-a, 97,640 ($mol^{-1}cm^{-1}$) at 470 nm for Chl-b, 141,000 ($mol^{-1}cm^{-1}$) at 453 nm for β-carotene and 60,000 ($mol^{-1}cm^{-1}$) at 535 nm for betanin [7, 10, 15].

Table 1

C1 concentrations (μg/cc) for the chromophores of all plants in this investigation

Plant	**Chl-a**	**Chl-b**	**Carotene**	**Betanin**
Artemisia arborescens	14.45	9.07	4.58	6.97
Spinach	14.21	9.15	4.38	6.55
Sage	14.03	8.87	4.28	5.88
Chives	13.98	8.05	4.06	4.58
Mentha	13.97	8.54	4.16	3.48
Parsley	13.87	9.01	4.72	5.29
Celery	13.21	7.93	3.85	4.90
Dill	12.96	7.58	3.75	3.37
Mangold	12.93	7.71	3.95	5.65
Beet Greens	12.81	7.88	3.85	4.52
Coriander	12.72	6.88	3.55	5.31
Rosemary	12.65	6.80	3.51	3.22
Lettuce	12.83	7.56	3.85	1.53
Leek	12.60	6.76	3.56	2.39
Green cabbage	12.21	6.46	3.39	1.80
Rocket	12.10	6.80	3.38	3.52
Basil	12.04	6.76	3.39	3.32
Green onion	11.89	6.31	3.31	2.15
Sorrel	11.41	6.00	3.13	0.88
Red cabbage	9.07	5.09	2.44	3.76

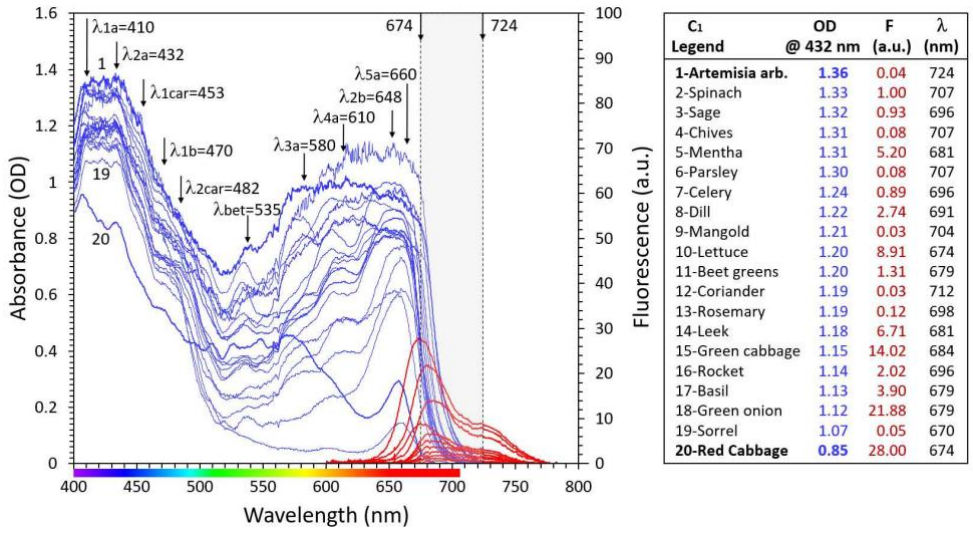

Fig. 1. Optical absorption spectra (blue curves) and fluorescence spectra (red curves) of the as extracted solutions concentrations – C1 (9 – 15 μg/cc). The *OD* in the annexed table is given in decreasing order and together with the black numbers above or below the absorption curves aid in the identification of the specific plant absorbance curve.

Figure 1 shows the typical optical absorbance spectra (blue curves) obtained for all plants of the as-extracted concentrations C1 in the spectral range of 400 to

800 nm. The Chl-a calculated concentrations C1 as seen from Table 1 are in the range of 9–15 μg/cc. The right annexed table in Figure 1 shows the specific optical densities at 432 nm for all samples. The *OD* values are proportional to the concentrations of Chl-a. In the annexed table, *F* denotes the peak fluorescence of every specific plant and λ is the corresponding wavelength.

The absorption spectra have very similar shapes for the various plant solutions, though they mostly show grossly resolved spectral peaks for the C1 concentrations, especially in the blue spectral band. The pointed arrows at 410 nm, 432 nm, 580 nm, 610 nm, and 660 nm correspond to the well-established Chl-a optical absorption lines [10]. The arrows positioned at about 470 nm and 648 nm pertain to Chl-b and the main β-carotene absorption lines also appear at about 453 nm and 482 nm. A smaller betanin peak is observed at about 535 nm [7, 15]. The red curves on the right depict the fluorescence spectra of the plant solutions samples excited at 405 nm. One may observe that the fluorescence curves show for all plants a leading Gaussian peak located in the red spectrum followed by a decreasing shoulder in the near-infrared (NIR). The gray shading in the 674–724 nm band specifies the wavelength range throughout which the particular Gaussian peak wavelengths are scattered for the different plants at C1 concentration. Most plants exhibit at these high pigment concentrations, quite low fluorescence, typically much less than 15 a.u. apart from 2 exceptions (green onion and red cabbage). This result corresponds to the observation that at high chlorophyll concentration, the fluorescence is quenched [10]. The low intensity fluorescence values obtained for the higher C1 concentrations can be attributed to several quenching processes such as scattering due to aggregation and photobleaching [17, 18] detailed later in the discussion.

In Figure 2, we present the optical absorbance spectral plots (blue curves) and in the annexed table, the specific optical density (*OD)* at 432 nm for the plants solutions diluted to the so called “optimum concentrations” Copt, typically obtained for Chl-a in the range 1–7 μg/cc. The Copt concentrations samples are defined as those providing the highest fluorescence values *F*, as seen in the annexed table. The *OD* values in the table are arranged here also in decreasing order for all plants. As compared to Figure 1, the typical Chl-a absorption spectral peaks in the blue spectrum can be observed here to possess a much better resolution.

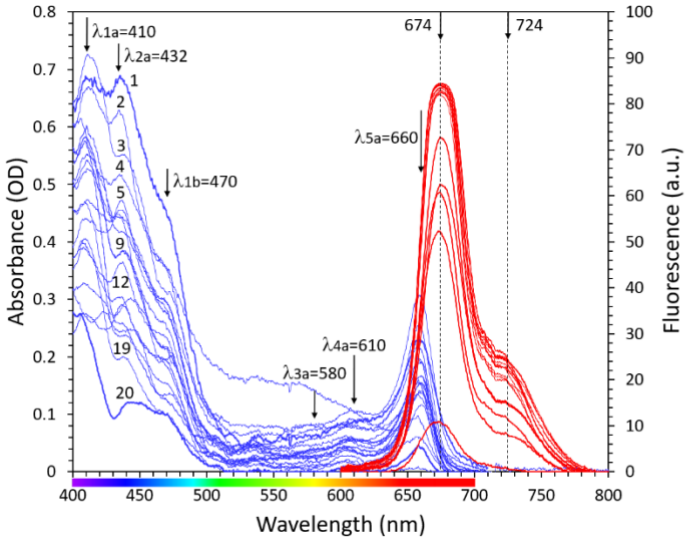

Copt Legend	OD @ 432 nm	F (a.u.)
1-Green onion	**0.68**	72.71
2-Green Cabbage	0.62	83.59
3-Basil	0.55	83.95
4-Red Cabbage	0.51	52.35
5-Parsley	0.45	82.35
6-Rosemary	0.45	82.84
7-Leek	0.45	62.50
8-Lettuce	0.44	81.98
9-Mentha	0.42	83.37
10-Beet greens	0.37	83.91
11-Celery	0.37	82.99
12-Coriander	0.35	84.36
13-Artemisia arb.	0.30	84.50
14-Chives	0.28	84.52
15-Rocket	0.27	60.87
16-Sage	0.26	84.09
17-Sorrel	0.25	10.98
18-Dill	0.24	84.12
19-Spinach	0.20	84.38
20-Mangold	0.10	82.56

Fig. 2. Optical absorption spectra (blue curves) and fluorescence spectra (red curves) of all plant solutions at optimal Chl-a concentrations – Copt (1–7 µg/cc). The *OD* decreasing values in the table together with the black numbers above the absorption curves aid to identify the specific plant curve.

The fluorescence spectra obtained here also exhibit a higher fluorescence, ~85 a.u., when compared to the as-extracted C1 concentration samples. Also, the fluorescence Gaussian peaks' wavelengths are blue-shifting from the scattered spectral lines seen in Figure 1, converging to exactly 674 nm for all plants. This blue shift due to dilution is about 5 – 50 nm towards the spectral line of 674 nm, as can be gathered from the λ column in the table of Figure 1. The small shoulder fluorescence peak at 724 nm in the near-infrared (NIR) also increases by dilution like the leading Gaussian peak but remains unshifted and stays locked at 724 nm for all samples' concentrations.

In Figure 3, we finally present the optical absorption spectra (blue curves) of all plant solutions for the lowest concentration case, C8 (0.003–0.6 µg/cc), obtained after 7 dilutions.

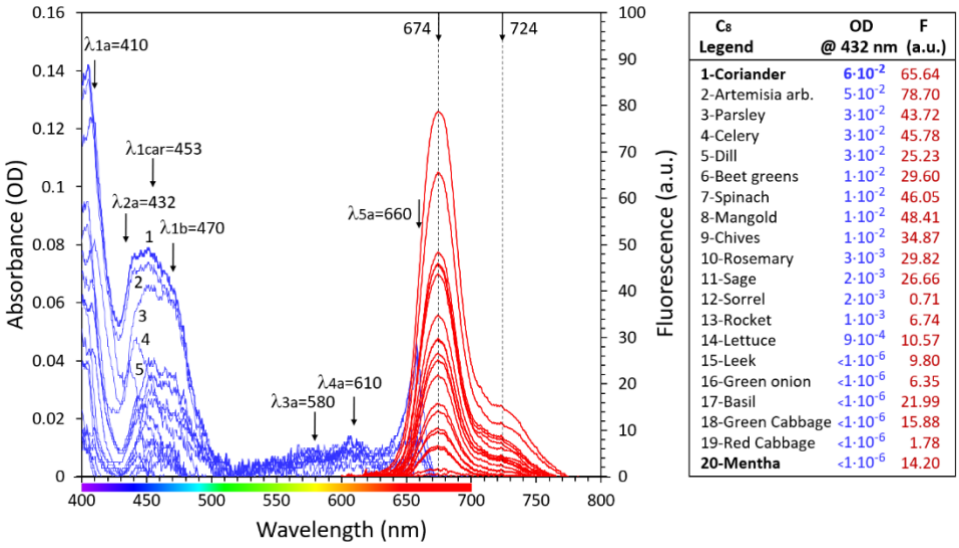

C8 Legend	OD @ 432 nm	F (a.u.)
1-Coriander	$6 \cdot 10^{-2}$	65.64
2-Artemisia arb.	$5 \cdot 10^{-2}$	78.70
3-Parsley	$3 \cdot 10^{-2}$	43.72
4-Celery	$3 \cdot 10^{-2}$	45.78
5-Dill	$3 \cdot 10^{-2}$	25.23
6-Beet greens	$1 \cdot 10^{-2}$	29.60
7-Spinach	$1 \cdot 10^{-2}$	46.05
8-Mangold	$1 \cdot 10^{-2}$	48.41
9-Chives	$1 \cdot 10^{-2}$	34.87
10-Rosemary	$3 \cdot 10^{-3}$	29.82
11-Sage	$2 \cdot 10^{-3}$	26.66
12-Sorrel	$2 \cdot 10^{-3}$	0.71
13-Rocket	$1 \cdot 10^{-3}$	6.74
14-Lettuce	$9 \cdot 10^{-4}$	10.57
15-Leek	$<1 \cdot 10^{-6}$	9.80
16-Green onion	$<1 \cdot 10^{-6}$	6.35
17-Basil	$<1 \cdot 10^{-6}$	21.99
18-Green Cabbage	$<1 \cdot 10^{-6}$	15.88
19-Red Cabbage	$<1 \cdot 10^{-6}$	1.78
20-Mentha	$<1 \cdot 10^{-6}$	14.20

Fig. 3. Optical absorption spectra (blue curves) and fluorescence spectra (red curves) of all plant solutions for the lowest Chl-a concentrations case – C8 (0.003–0.6 µg/cc). The *OD* decreasing values in the table together with the black numbers above the absorption curves aid in identifying the specific plant optical absorption curve.

The *OD* values shown here are at least 3 times lower than in Figure 2, and about 10 times lower than for the C1 values, but the spectra still show the presence of mainly the Chl-a chromophores. The absorption spectra and the adjacent table show that as the plant solutions are diluted beyond their optimum concentration Copt, the chromophores' sources of the absorption maxima (blue lines) become less clear in the 400–500 nm range. This makes it more difficult to distinguish between the peaks' contributions of Chl-a at 432 nm, β-carotene at 453 nm, and Chl-b at 470 nm. The fluorescence amplitudes (red curves) are distributed here in the wide range (0.71–78.70 a.u.), but still clearly show the Gaussian peaks at 674 nm and the shoulder peak is still frozen at 724 nm. This means that even in the low Chl-a concentration case, there are enough pigments left in the solutions to produce a significant fluorescence.

DETAILS OF THE CONCENTRATION EFFECT ON THE SOLUTIONS SPECTRAL CHARACTERISTIC PARAMETERS

Our analysis of the positions and amplitudes of the absorption peaks and fluorescence spectra depicted in Figures 1–3 suggests that Chl-a is the primary chromophore contributor to the samples' fluorescence. The additional dilution of solutions with ethanol, giving the spectra in Figures 2–3, led to an absolute increase in the fluorescence intensity due to less absorption losses of the emitted photons in the solutions' irradiated volume. It also resulted in a better resolution of the optical absorbance spectral peaks compared to the as-extracted samples' spectra depicted in Figure 1. The better resolution of the Chl-a absorption peaks is believed to occur due to the relatively stronger absorption of Chl-a chromophores in the volume during dilution, as compared to the other less prevalent pigments, emphasizing even more the dominant influence of the Chl-a molecules at lower concentrations. The fluorescence small shoulder peak in the near-infrared (NIR) band also increases during dilution to the optimized concentration Copt, following the leading Gaussian peak behavior, though its wavelength location remains unshifted at ~ 724 nm for all concentrations (Figures 1–3). This is consistent with the results published in [11, 19], which attributes the shoulder fluorescence appearance to the mechanism of re-absorption of the Gaussian peak fluorescence by nearby molecules and the subsequent emission of photons in the NIR. The decreasing fluorescence of the diluted solutions in Figure 3 compared to Figure 2 can be attributed to the excessive depletion and rarefication of the chromophore concentration due to the dilution procedure beyond the optimal concentration. This overall diminishing fluorescence is similar to that observed for the high concentration case C1, but for C8 it is due to the rarefication mechanism while in the C1 cases it is due to excessive absorption and scattering.

In Figure 4, we present the absorbance ratio Ra = A432/A660 at 432 nm and 660 nm for 8 representative plant solutions. The general increasing trend of this ratio above $Ra > 1$ as a function of dilution steps can be explained by considering how the dilution is affecting the absorption curves from purely volume geometrical considerations.

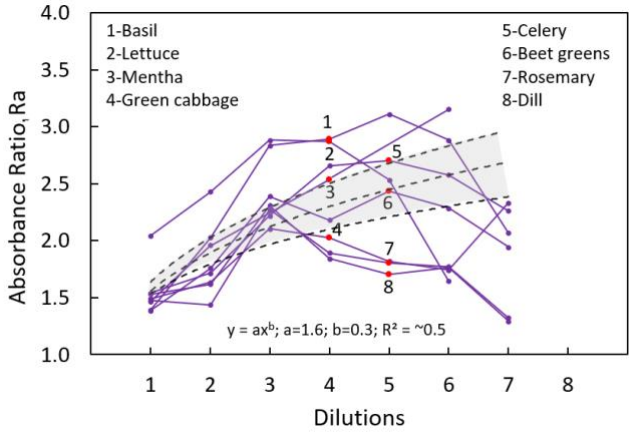

Fig. 4. Absorbance ratio *Ra* vs. dilutions steps for the 8 plants denoted in the inserts. Red dots represent the optimized diluted concentrations where the fluorescence is maximal for each plant.

Red light can penetrate further inside a chlorophyll-a solution than blue light. This means that blue light is absorbed mainly at the entrance of the cell, and thus relatively fewer molecules contribute to the blue absorbance signal at the photodetector side than red photons. Hence, as the concentration of the solution is reduced, the blue photons penetrate to longer distances and contribute relatively more to the measured absorbance than before the dilution. Eventually, a balance is reached, and the absorbance from both blue vs. red light is maximized. This balance occurs in the figure at the red points, which represent the optimized concentrations. The shaded area between the 3 dotted curves is obtained by fitting the absorbance ratio to a power law $y = ax^b$ for the specific plants 1, 5, 6 and represents the behavior of *Ra* vs. the dilution steps. The increased absorption pathlength of the blue photons by dilution leads thus to an increase in the ratio *Ra* as concentration decreases. This is the general trend observed in Figure 4 and this effect has been reported in other studies as well [3, 14]. Further details of the photoexcitation processes involved during dilution are deduced from Figures 5a–5b displaying the linear-log plot of the fluorescence spectra and peak wavelength respectively of the Chl-a concentrations C1–C8 for all 20 plants.

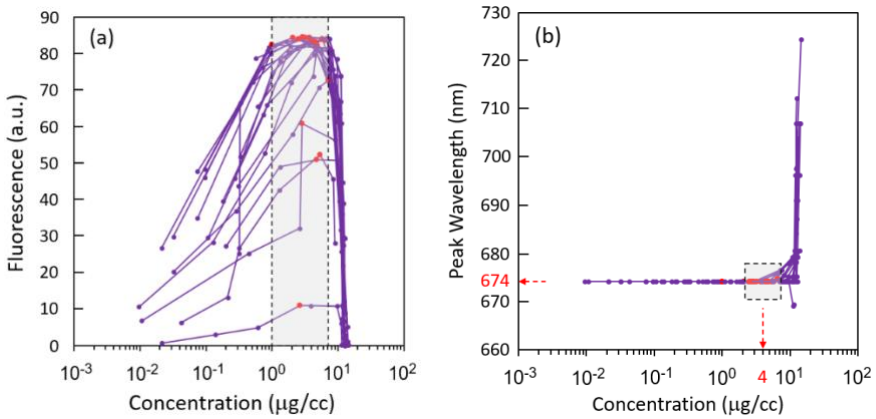

Fig. 5. Linear-log plots of (a) fluorescence intensity and (b) wavelength of the optimal fluorescence peak vs. Chl-a concentration for all plants investigated at all concentrations C1–C8. The red points indicate the optimal concentration obtained for each plant.

The fluorescence intensity plateau at ~85 a.u. in Figure 5a is obtained for most plants at their optimized diluted Chl-a concentration Copt, in the range of 1–7 µg/cc. The fluorescence plots of the plant solutions samples in Figure 5a show that the curves decrease sharply at both concentration extremal zones due to aggregation, agglomeration, or dilution mechanisms of the molecules. The smaller fluorescence obtained for the highly concentrated samples is caused by the stronger optical absorption and scattering, while at the very diluted end it is due to the excessive depletion of the chromophores in the solutions. It was mentioned also in [19] that when the concentration of Chl-a molecules decreases by dilution, the Gaussian fluorescence peak undergoes a blue shift towards the 674 nm wavelength. This outstanding phenomenon is clearly observed in Figure 5b, which plots the Gaussian peak wavelength vs. concentration for all the various plants solutions. Since this peak spectral line at 674 nm was obtained for all 20 plants investigated, it may be called the 'intrinsic' or natural Chl-a fluorescing line. This is a wavelength which characterizes the fluorescence of the unperturbed Chl-a molecules in ethanol solutions as realized from comparing the results in Figure 1 with Figures 2 and 3. The blue shift stops at a mean critical concentration of ~ 4 µg/cc, when the aggregated Chl-a molecules are assumed to disperse into isolated monomer molecules surrounded only by ethanol molecules. For further dilutions, the peak remains fixed at 674 nm. Interestingly, the shoulder small peak at 724 nm is also kind of a specific natural wavelength characterizing the re-emitted fluorescence from the neighboring Chl-a molecules. However, unlike the Gaussian primary fluorescence peak, it does not shift with dilution and stays fixed for all plants and all concentrations.

The ratio between the Gaussian peak fluorescence at 674 nm and the shoulder smaller peak fluorescence at 724 nm, i.e., F_{GS}, is given next in Figure 6. It shows that although the shoulder peak fluorescence intensity increases like the Gaussian fluorescence peak with dilution, F_{GS} increases even steeper beyond the optimal

concentration. A similar plot was observed in another work [12]. This can be understood by realizing that the self-absorption mechanism at 674 nm and re-emission of photons at 724 nm becomes less dominant when the concentration of the molecules becomes much lower than Copt. Thus, when a Chl-a molecule emits a photon of about 674 nm energy, this photon can be absorbed by a neighboring Chl-a molecule, which can then emit another photon of lower energy. This lossy energy process can continue, with each successive photon being emitted at a longer wavelength. The extended spectral shoulder of the fluorescence into the NIR is then likely due to the emission of photons at these longer wavelengths.

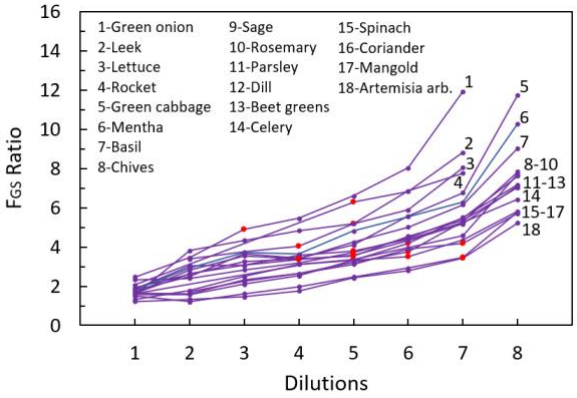

Fig. 6. Fluorescence ratio F_{GS} vs. dilutions for 18 of the plants denoted in the inset. The red dots represent the optimized diluted concentrations where the fluorescence is maximal for each plant.

In Figure 7, showing the Gaussian fluorescence bandwidth (*BW*) vs. Chl-a concentration, four distinct mechanisms can be suggested to occur in the M1–M4 zones. The first mechanism, effective at M1, is the behavior of the highly concentrated Chl-a solutions. Due to various photo-excitation processes, the chromophore particles may become photo-bleached, photo-aggregated, aggregated, and agglomerated [17, 18], all of which are characterized by wide spectral bandwidths. Photobleaching usually lowers the optical density and also the fluorescence intensity of the solutions during irradiation [12, 18]. Previous work in our laboratory has demonstrated large differences in the photosensitivity of the monomeric versus the aggregated pigments [17, 18]. We have also observed photo-aggregation processes in colloid solutions accompanied by photo-deposited layers and turbidity in the cuvettes [17, 18]. Thus, preferential photobleaching of monomers versus aggregates and the competition between these processes may indeed affect fluorescence efficacy.

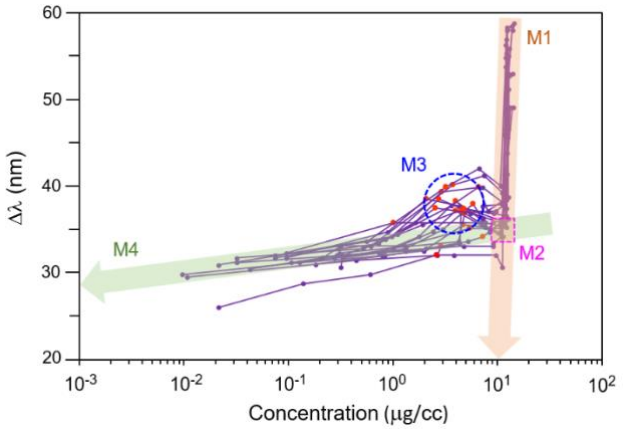

Fig. 7. Linear-log plot of the Gaussian fluorescence bandwidth vs. Chl-a concentration for all plants. The dotted blue circle encircling the red points denotes the optimized solutions zone while the smaller dotted purple square the zone where the slope becomes shallower.

From point M1, the Gaussian peak bandwidth (*BW*) decreases steeply as the concentration of Chl-a is diluted from 15 μg/cc to about 4 μg/cc. This effect can be explained by assuming that when the Chl-a molecules are in close proximity, their excitonic coupling is enhanced, leading to a more efficient energy transfer between neighboring molecules, resulting in a broadening of the fluorescence bandwidth. As the solution is diluted towards M2, the agglomerated molecules undergo a dispersion process, eventually becoming mostly monomers. The dotted purple square at M2 indicates where this process starts. Thus, when the Chl-a molecules are dispersed or de-aggregated in a diluted solution, their excitonic coupling decreases, leading to a narrower fluorescence bandwidth. Alternatively, the Förster resonance energy transfer (FRET) mechanism can also explain this behavior [6, 13]. However, since the Chl-a molecules in solution are not tightly packed together like in leaves, the dephasing of the emission spectrum is more likely due to one of the other mechanisms mentioned above. The small recurring increase in *BW* from the M2 to M3 zone at around 4 μg/cc can be explained by another effect. As the concentration of chlorophyll decreases below M2, the interaction zone between the photons and molecules becomes greater for the shoulder spectra fluorescing photons. This is because the shoulder wavelengths photons with a lower energy than the Gaussian peak photons, possess a longer penetration depth. The expansion of the local zone for the shoulder photons means that more shoulder photons can be absorbed by the remaining chlorophyll molecules, thus increasing their collection efficiency. This increased collection efficiency of the longer wavelength shoulder photons in the detector leads to an overall increase in the Gaussian bandwidth causing the "hilly" curves shapes seen near point M3. Continuing from point M3 to further dilutions beyond the optimum level Copt decreases again the interaction between the molecules in the excited zone. This effect reduces both the Gaussian fluorescence and simultaneously its bandwidth, although with a shallower slope since the

molecules are then already de-aggregated monomers. Then in the fourth zone, towards M4, the shallower slope of the *BW* is due to the excessive reduction of the monomers concentration in the solution. Now, from the shallower slope plot the ideal monochromatic bandwidth value of the Chl-a molecule fluorescence line at 674 nm can be obtained by extrapolating the curves from the M2–M3 zone towards the M4 zone. This gives for the single Chl-a molecule of concentration (~1.5×10^{-15} μg/cc) a theoretical bandwidth of 14 nm.

THE ENERGY MODEL OF THE SPECTRAL BANDS TRANSITIONS

We can now allocate from the measured absorption spectra for all plants the *B* and *Q* absorption bands of the Chl-a molecule along with their corresponding energy bands *Sn*. These absorption and corresponding fluorescing bands have been discussed previously in many published papers [8, 21, 22, 25]. We include here also the third absorption band designated by Qx^+ for the Chl-a molecule accounting for the small absorption peak at λa=580 nm, clearly seen in Figures 1–3. This peak, which can be observed also in the spectral plots of many other published works of Chl-a, is rarely mentioned and discussed explicitly in only a few [21, 25]. Concluding, the absorption peaks at specific λa occurring in the *Q* and *B* bands can be associated with the lowest five energy levels of the molecular bands *Sn* as follows: 660 nm with *S*1, 610 nm with *S*2, 580 nm with $S2^+$, 432 nm with *S*3 and 410 nm with *S*4. These wavelengths correspond to the zero energy level in each of the specific *Sn* bands as shown in Table 2.

Table 2 shows the zero energy levels in each *Sn* band from the *S*0 ground level, as measured by our experimental spectra and compared to similar values from other sources in the literature [8, 21, 22, 25].

Table 2
S bands parameters

Bands	***Sn***	**Other sources [8, 21, 22, 25]**		**This work**		
B, Q		**λa (nm)**	***E* (eV)**	**λa (nm)**	***E* (eV)**	**$\Delta\lambda a$ (nm)**
By	*S*4	400–420	3.1–2.9	**410**	3.02	10
Bx	*S*3	420–440	2.9–2.8	**432**	2.86	9
Qx^+	$S2^+$	498–588	2.4–2.1	**580**	2.14	60
Qx	*S*2	600–640	2.0–1.9	**610**	2.03	20
Qy	*S*1	650–680	1.9–1.8	**660**	1.88	33

The absorption bandwidth $\Delta\lambda a$ for every energy band *S*1–*S*4 is estimated from the points where the absorbance value from the corresponding peak shows a turning or saddle point at the adjacent local minima. We conclude the spectral transitions in our plants by presenting the Jablonski diagram in Figure 8, after [21], which schematically shows the excitation, absorption, and fluorescence processes for a

typically chosen plant, parsley. The diagram provides both energy and wavelength scales for the absorption spectra (green curve) and fluorescence emission (red curve). The excitation line 405 nm of the violet-blue LED source used in our investigation, and for comparison also green and red-light excitation lines, are also drawn in the diagram.

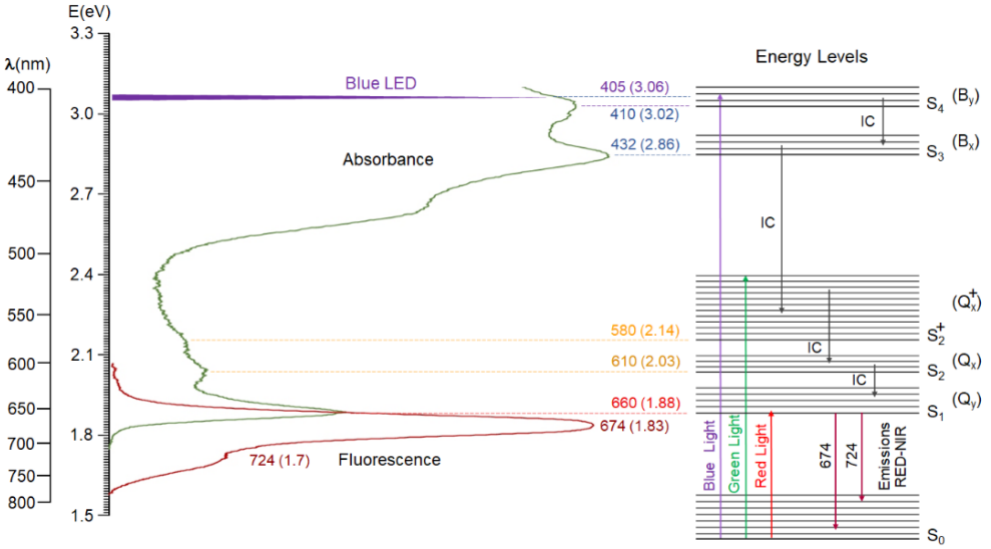

Fig. 8. Jablonski energy diagram for Chl-a in an optimized parsley solution. The absorption and fluorescent spectra show the natural spectral peaks of Chl-a with the fluorescence lines at 674 and 724 nm. The specific wavelengths are given in nm with corresponding energies eV in the parentheses.

The right-hand side of the diagram shows the different singlet states – *Sn* of the Chl-a molecule. The *S*0 state is the molecular ground state, and the *S*1 state is the first singlet excited state. The *S*2–*S*4 levels denote the higher excited states. The *S*1 → *S*0 transitions are the final and most important ones responsible for the red fluorescence of Chl-a. Excited electrons from the other *Sn* > *S*1 bands rapidly relax to *S*1 *via* vibrational non-radiative energy dissipation and internal conversion (*IC*) transitions. The excited Chl-a electrons by the 405 nm radiation propagate serially down the energy levels of Chl-a, as seen in the Jablonski diagram, finally populating the singlet band *S*1. The Gaussian fluorescence peak at 674 nm, observed in our research for all plant solutions and denoted as the intrinsic Chl-a fluorescence line, appears in the diagram as a transition from the *Qy* band level to some low vibration level in the *S*0 band. As mentioned previously, the small spectral peak in the NIR at 724 nm appears to originate from self-absorption of the monomers, also creating a vibronic band shoulder after the Gaussian due to the presence of vibrational modes in the pigment molecules, causing the fluorescence energy to be spread out over a range of wavelengths in the NIR.

CONCLUSIONS

This study investigated in detail the absorption and fluorescence spectra of chlorophyll solutions extracted from 20 various edible plants by extra dilution in ethanol. The results showed that all plants exhibited several common spectral characteristics. Two broad emission peaks were observed for all Chl-a concentrations, ranging from 0.003 to ~15 μg/cc. The leading Gaussian peak fluorescence of all plant solutions shifted towards the intrinsic spectral emission line of 674 nm during dilution, by 5 to 50 nm. The Gaussian peak bandwidth decreased at the same time by dilution from 60 to 30 nm. A small, localized peak of the fluorescence shoulder in the NIR region was observed for all concentrations, which can be attributed to the smaller secondary re-emission fluorescence of the chlorophyll-a molecule at 724 nm. These findings suggest that the spectral fluorescence properties of chlorophylls can be sensitively tuned by controlling the concentration in a suitable solvent, such as ethanol. This method could be practically useful for bio-diagnostics in various environments, as well as in applications such as fluorescent quantum dots, lasers, and medical sensors.

Acknowledgements. The authors wish to thank Prof. Dr. Hartmut K. Lichtenthaler from Karlsruhe Institute of Technology for helpful suggestions during this investigation.

REFERENCES

1. CAI, J.Q., X.M. LIU, Z.J. GAO, L.L. LI, H. WANG, Chlorophylls derivatives: Photophysical properties, assemblies, nanostructures and biomedical applications, *Mat. Today*, 2021, **45**, 77–92.
2. CALOGERO, G., I. CITRO, C. CRUPI, G. CARINI JR., D. ARIGO, G. SPINELLA, A. BARTOLOTTA, G. DI MARCO, Absorption spectra, thermal analysis, photoelectrochemical characterization and stability test of vegetable-based dye-sensitized solar cells, *Optical Materials*, 2019, **88**, 24–29.
3. CARTER, G.A., B.A. SPIERING, Optical properties of intact leaves for estimating chlorophyll concentration, *J. Environ. Qual*., 2002, **31**, 1424–1432.
4. CHEN, Y.C., Q. CHEN, X. FAN, Optofluidic chlorophyll lasers, *R. Soc. Chem*., 2016, **16**, 2228–2235.
5. FARALONI, C., I. CUTINO, R. PETRUCCELLI, A.R. LEVA, S. LAZZERI, G. TORZILLO, Chlorophyll fluorescence technique as a rapid tool for in vitro screening of olive cultivars (*Olea europaea* L.) tolerant to drought stress, *Environmental Exp. Botany*, 2011, **73**, 49–56.
6. GRIMM, B., R.J. PORRA, W. RUDIGER, H. SCHEER, *Chlorophylls and Bacteriochlorophylls, Biochemistry, Biophysics, Functions and Applications*, Springer, Netherlands, 2006.
7. JEFFREY, S.W., *Preparation of Chlorophyll Standards. Phytoplankton Pigments in Oceanography: Guidelines to Modern Methods*, S.W. Jeffrey, R.F.C. Mantoura, S.W. Wright eds, UNESCO Publishing, Paris, 1997, pp. 207–238.
8. KARCZ, D., Lessons from chlorophylls: modifications of porphyrinoids towards optimized solar energy conversion, *Molecules*, 2014, **19**, 15938–15954.

9. LICHTENTHALER, H.K., F. BABANI, M. NAVRATIL, C. BUSCHMANN, Chlorophyll fluorescence kinetics, photosynthetic activity, and pigment composition of blue-shade and half-shade leaves as compared to sun and shade leaves of different trees, *Photosynth. Res*., 2013, **117**, 355–366.
10. LICHTENTHALER, H.K., Chlorophylls and carotenoids: pigments of photosynthetic bio membranes, *Meth. Enzymol*., 1987, **148**, 350–382.
11. LICHTENTHALER, H.K., U. RINDERLE, The role of chlorophyll fluorescence in the detection of stress conditions in plants, *CRC Critical Reviews in Analytical Chemistry*, 1988, **19**, Supplement 1, S29–S85.
12. LICHTENTHALER, H.K., R. HAK, U. RINDERLE, The chlorophyll fluorescence ratio F690/F730 in leaves of different chlorophyll content, *Photosyn. Research*, 1990, **25**, 295–298.
13. LINDSEY, J.S., The fluorescence quantum yield parameter in Forster resonance energy transfer (FRET) – Meaning, misperception, and molecular design, *Chem. Phys. Rev*., 2021, **2**, 011302.
14. MELER, J., M. OSTROWSKA, D. FICEK, A. ZDUN, Light absorption by phytoplankton in the southern Baltic and Pomeranian lakes: mathematical expressions for remote sensing applications, *Oceanologia*, 2017, **59**, 195–212.
15. OBI, K., L. FROLOVA, P. FUIERER, Preparation and performance of prickly pear (*Opuntia phaeacantha*) and mulberry (*Morus rubra*) dye-sensitized solar cells, *Solar Energy*, 2020, **208**, 312–320.
16. PEDROS, R., I. MOYA, Y. GOULAS, S. JACQUEMOUD, Chlorophyll fluorescence emission spectrum inside a leaf, *Photochem. Photobiol. Sci*., 2008, **7**, 498–502.
17. PELED, A., N. MIRCHIN, Liquid phase photodeposition processes from colloid solutions, In: *Photo-Excited Processes, Diagnostics and Applications (PEPDA): Fundamentals, Applications and Advanced Topics*, A. Peled Ed., Kluwer Academic Publishers, Boston, 2003, pp. 251–276.
18. PELED, A., Y. DROR , I. BAAL-ZEDAKA, A. PORAT, N. MIRCHIN, I. LAPSKER, Photobleaching and photodeposition in a chlorophyll based solution, *Synth. Metals*, 2000, **115**, 167–171.
19. POPESCU, S.A., A. PELED, Optimized RED spectral band fluorescence of edible plants leaves extracts, *Applied Surface Science Advances*, 2023, **13**, 100385 (1–5).
20. PUCCI, C., C. MARTINELLI, A. DEGL'INNOCENTI, A. DESII, D.D. PASQUALE, G. CIOFANI, Light-activated biomedical applications of chlorophyll derivatives, *Macromol. Biosci*., 2021, **21**, 2100181 (1–19).
21. RATSEP, M., J.M. LINNANTO, A. FREIBERG, Higher order vibronic sidebands of chlorophyll a and bacteriochlorophyll a for enhanced excitation energy transfer and light harvesting, *J. Phys. Chem.*, 2019, **B 123**, 7149–7156.
22. SCHMIDT, W., Luminescence of organic molecules theory and analytical applications in photosynthesis in applications of chlorophyll fluorescence, In: *Photosynthesis Research, Stress Physiology, Hydrobiology and Remote Sensing*, H.K. Lichtenthaler, ed., *Kluwer Academic Publishers*, London, 1988, 210-216.
23. SEMERARO, P., G. CHIMIENTI, E. ALTAMURA, P. FINI, V. RIZZI, P. COSMA, Chlorophyll a in cyclodextrin supramolecular complexes as a natural photosensitizer for photodynamic therapy (PDT) applications, *Materials Science & Engineering*, 2018, **C85**, 47–56.
24. SHEN, J.R., K. SATOH, S.I. ALLAKHVERDIEV, Photosynthesis: Molecular approaches to solar energy conversion, *Advances in Photosynthesis and Respiration*, 2021, **47**, 133-162.
25. SONG, Y., A. SCHUBERT, E. MARET, R.K. BURDICK, B.D. DUNIETZ, E. GEVA, J.P. OGILVIE, Vibronic structure of photosynthetic pigments probed by polarized two-dimensional electronic spectroscopy and ab initio calculations, *Chem. Sci*., 2019, **10**, 8143–8153.
26. TANIGUCHI, M., J.S. LINDSEY, Absorption and fluorescence spectral database of chlorophylls and analogues, *Photochemistry and Photobiology*, 2021, **97**, 136–165.
27. ZVEZDANOVIC, J., T. CVETIC, S. VELJOVIC-JOVANOVIC, D. MARKOVIC, Chlorophyll bleaching by UV-irradiation in vitro and in situ: Absorption and fluorescence studies, *Radiation Physics and Chemistry*, 2009, **78**, 25–32.